THE JOURNAL OF PHYSICAL CHEMISTRY Letters

Letter

pubs.acs.org/JPCL

Robust Superlubricity in Graphene/*h*-BN Heterojunctions

Itai Leven, Dana Krepel, Ortal Shemesh, and Oded Hod*

Department of Chemical Physics, School of Chemistry, The Raymond and Beverly Sackler Faculty of Exact Sciences, Tel-Aviv University, Tel-Aviv 69978, Israel

Supporting Information

ABSTRACT: The sliding energy landscape of the heterogeneous graphene/*h*-BN interface is studied by means of the registry index. For a graphene flake sliding on top of *h*-BN, the anisotropy of the sliding energy corrugation with respect to the misfit angle between the two naturally mismatched lattices is found to reduce with the flake size. For sufficiently large flakes, the sliding energy corrugation is expected to be at least an order of magnitude lower than that obtained for matching lattices regardless of the relative interlayer orientation. Therefore, in contrast to the case of the homogeneous graphene interface where flake reorientations are known to eliminate superlubricty, here, a stable low-friction state is expected to occur. Our results mark heterogeneous layered interfaces as promising candidates for dry lubrication purposes.

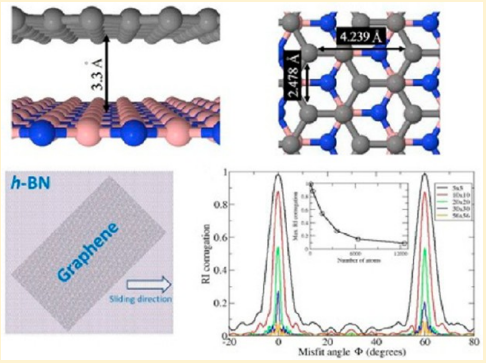

SECTION: Physical Processes in Nanomaterials and Nanostructures

Homogeneous layered materials such as graphite, hexagonal boron nitride (*h*-BN), and 2*H*-molybdenum disulfide and its fullerene derivatives may serve as solid lubricants at confined nanoscale junctions where traditional liquid-phase lubricants become too viscous.[1−9] The excellent tribological properties that these materials present stem from their anisotropic crystal structure consisting of strong covalent intralayer bonding and weaker interlayer dispersive interactions.[10] As a consequence, adjacent layers may slide on top of each other while overcoming relatively low energetic barriers.

Recently, the wearless friction between a nanoscale graphene flake and a graphite surface was studied experimentally as a function of the misfit angle between the two surfaces.[11,12] The measured friction forces were found to range from moderate to vanishingly small depending on the degree of commensurability between the lattices of the flake and the underlying surface. The ultralow friction state occurring at incommensurate configurations, often termed a superlubric state,[13−16] is of high interest both from the basic scientific perspective of nanotribology[17−25] and in light of the potential technological opportunities that it carries.[26−29]

Computational studies based on the Tomlinson model[30] and its extensions were able to capture the main physical features appearing in the observed frictional behavior of the graphitic system.[31] It was shown that the flakes dock on the surface by a delicate balance between van der Waals (vdW), electrostatic, and Pauli interactions.[32−36] Here, a universal character of vdW interactions was predicted for the interlayer binding in many layered materials including *h*-BN and graphite.[37] Nevertheless, such dispersion interactions were shown to have a marginal effect on the interlayer sliding corrugation.[32,33] Upon sliding, the dynamical stability of the superlubric state obtained for a single graphene flake[38] and multiple flakes confined between infinite graphene layers[39] was investigated, and it was shown that for relatively small flakes sliding on top of an extended graphene surface, torque-induced flake reorientations during the lateral motion may eliminate superlubricity of the homogeneous interface.[40] This is in contrast to the case of multiwalled carbon nanotubes where lattice incommensurability was shown to induce stable and extremely small shear strengths.[41] Furthermore, recent atomistic simulations[42] indicate that surface deformation may enhance friction when suspended few-layer graphene is subject to tip scanning, in agreement with experimental observations.[6] This is further supported by a recent study showing that multilayered graphene and *h*-BN nanoribbons bend and kink with no evident interlayer sliding.[43]

In the present study, the superlubric state occurring at the heterogeneous interface of graphene and *h*-BN is investigated. This system, which has recently attracted attention in the context of its electronic properties,[44−56] is expected to present a robust superlubric behavior that is predicted to persist regardless of the relative flake−substrate orientation. We find that a key ingredient for this phenomenon is the naturally occurring lattice mismatch between the two materials resulting in low corrugation of the interlayer sliding energy landscape.

To perform our calculations, we utilize the recently developed registry index (RI) concept, which quantifies the degree of interlayer commensurability in layered materials via simple geometric considerations and relates it to the interlayer

Received: October 31, 2012
Accepted: December 9, 2012
Published: December 9, 2012

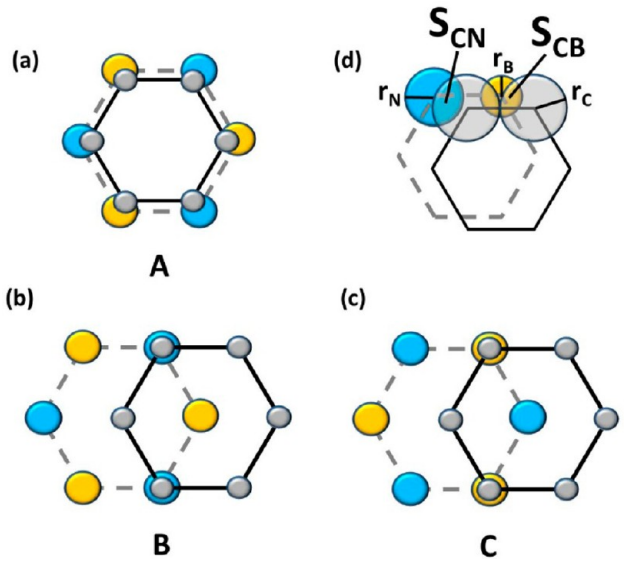

Figure 1. Schematic representation of high-symmetry stacking modes of graphene on *h*-BN: (a) the worst, A, stacking mode where the graphene and *h*-BN layers are fully eclipsed; (b) the B stacking mode where half of the carbon atoms reside atop of nitrogen atoms and the rest reside above hexagon centers of the *h*-BN hexagonal lattice; and (c) the optimal, C, stacking mode where half of the carbon atoms reside atop of boron atoms and the rest reside above hexagon centers of the *h*-BN hexagonal lattice. (d) Definition of the projected overlap areas used in the registry index calculation. As schematically depicted, we choose $r_C > r_N > r_B$ (see the main text for further details). Gray, orange, and blue circles represent carbon, boron, and nitrogen atoms, respectively. Notation of the different stacking modes is chosen to match that used in previous studies.[44].

sliding energy landscape.[33,57−59] This method is highly suitable to treat the short-range repulsive interactions between overlapping electron clouds responsible for the interlayer sliding energy corrugation.[33] Furthermore, it has been shown to accurately and efficiently reproduce the experimentally measured frictional behavior of the homogeneous graphitic interface[59] and is therefore chosen to study the sliding physics of the heterogeneous junction considered herein.

We start by defining the registry index for the graphene/*h*-BN interface. To this end, a strained unit-cell of the bilayer system is considered where the lattice vectors of the graphene and *h*-BN layers are taken to be identical (see the Supporting Information for the coordinates of this unit-cell). For this minimal unit-cell, three important high-symmetry stacking modes are identified (see Figure 1): (i) the A stacking mode where the two layers are fully eclipsed; (ii) the B stacking mode where one carbon atom resides atop of a nitrogen atom and the other carbon atom resides on top of the center of a *h*-BN hexagon; and (iii) the C stacking mode where one carbon atom resides atop of a boron atom and the other carbon atom resides on top of the center of a *h*-BN hexagon. The latter is known to be the optimal stacking mode[44,51] (in terms of energy) as it minimizes the interlayer repulsions between overlapping electron clouds. The A stacking mode, on the other hand, maximizes these repulsions and therefore represents the worst stacking mode of this system.

To define the RI, a circle is assigned to each atomic position on both layers, and the projected overlaps between circles belonging to the two adjacent layers are calculated. Two different types of overlaps are considered (see Figure 1d), (i) S_{CN}, the projected overlap between circles assigned to a nitrogen atom in the *h*-BN layer and circles associated with the carbon atoms of the graphene layer, and (ii) S_{CB}, the projected overlap between circles assigned to a boron atom in the *h*-BN layer and circles associated with the carbon atoms of the graphene layer. Noticing that at the optimal stacking mode S_{CB} is maximal and S_{CN} is minimal and that at the worst stacking mode both overlaps are of maximal value, we define the RI to be proportional to the sum of both overlaps, RI $\propto S_{CB} + S_{CN}$. With this definition the RI obtains a minimum value at the optimal stacking mode and a maximum at the worst staking mode, similar to the total energy of the bilayer system. Next, we normalize the RI to the range [0:1] in the following manner

$$\mathrm{RI}_{\mathrm{graphene}/h\text{-BN}} = \frac{(S_{CB} - S_{CB}^{C}) + (S_{CN} - S_{CN}^{C})}{(S_{CB}^{A} - S_{CB}^{C}) + (S_{CN}^{A} - S_{CN}^{C})}$$

where the value of 0 (1) is obtained at the optimal (worst) stacking mode. Here, S_{CB}^{A} and S_{CN}^{A} are the carbon−boron and carbon−nitrogen projected overlap areas at the worst (A) stacking mode and S_{CB}^{C} and S_{CN}^{C} are the carbon−boron and carbon−nitrogen projected overlap areas at the optimal (C) stacking mode. Finally, the circle radii are tuned to obtain a

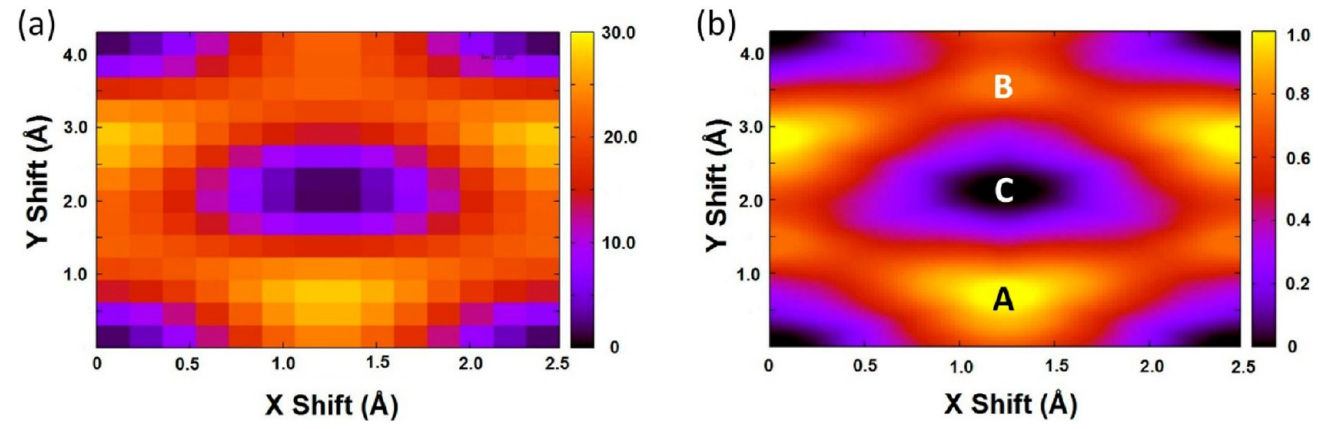

Figure 2. Graphene on *h*-BN interlayer sliding energy (a) and RI (b) landscapes calculated for the strained unit-cell. Total energy differences in the left panel (given in meV/unit-cell) were calculated using DFT at the HSE/6-31G* level of theory for a fixed interlayer distance of 3.3 Å (see the Supporting Information for further details). Capital letters in the right panel mark the location of the high-symmetry stacking modes depicted in Figure 1.

dx.doi.org/10.1021/jz301758c | *J. Phys. Chem. Lett.* 2013, 4, 115−120

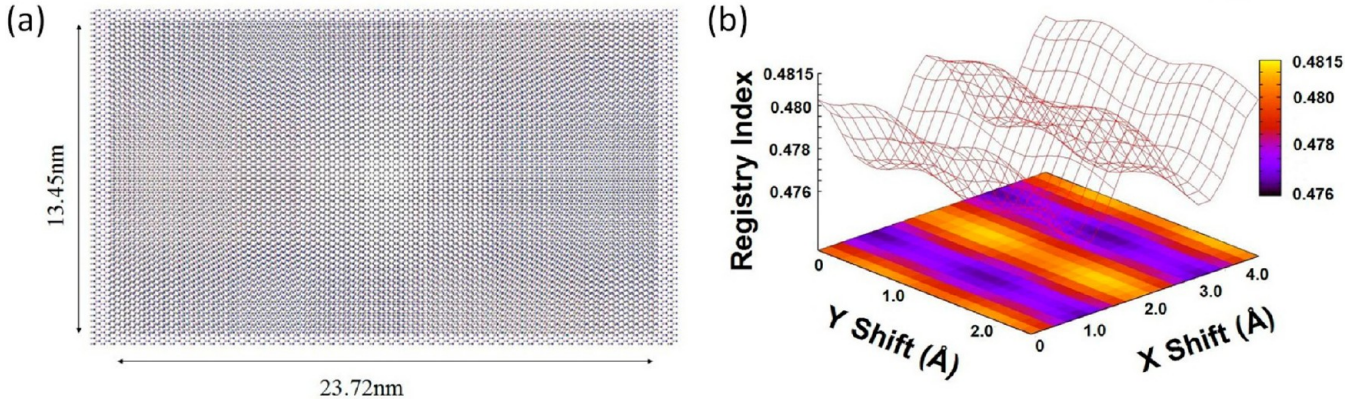

Figure 3. RI sliding surface of a supercell consisting of a 56 × 56 graphene unit-cell and a 55 × 55 *h*-BN unit-cell with L_{CC} = 1.42 Å and L_{BN} = 1.446 Å. (a) Schematic representation of the bilayer supercell showing the appearance of Moiré patterns due to the lattice mismatch between the graphene and *h*-BN unit-cells. (b) RI surface calculated for various interlayer stacking modes created by lateral shifts of the graphene layer with respect to the *h*-BN layer. The results are normalized to the size of the graphene flake such that a RI corrugation of 1 is obtained for a strained 56 × 56 graphene flake having no lattice mismatch with the underlying *h*-BN layer.

good fit between the RI predictions and first-principles calculations.

In Figure 2, we compare the RI surface calculated for different interlayer positions of the heterojunction and the sliding energy landscape calculated using the HSE screened hybrid functional approximation[60−62] within density functional theory (DFT) using the double-ζ polarized 6-31G* Gaussian basis set[63] as implemented in the Gaussian suite of programs[64] (further details regarding the DFT calculations can be found in the Supporting Information). This functional approximation has been successfully used to describe the intralayer structural and electronic properties of graphene and *h*-BN based materials.[65,66] To obtain good correspondence between the two surfaces, we choose $r_C = 0.5L_{CC}$, $r_N = 0.4L_{BN}$, and $r_B = 0.2L_{BN}$, where for the case of the strained unit-cell, the CC (L_{CC} and BN (L_{BN}) bond lengths are taken to be equal, $L_{CC} = L_{BN}$ = 1.431 Å. The agreement between the sliding energy landscape calculated from first-principles and the sliding RI surface presented in Figure 2 suggests that a simple scaling factor (of 28.2 meV/unit-cell in the present case) may be used to relate the results of the RI calculations to sliding energies obtained via advanced DFT methods for such systems.

The strained structure considered above for the definition of the RI was predicted to be plausible in an isolated graphene/*h*-BN bilayer system.[51] Nevertheless, for the case of graphene grown on the upper surface of bulk *h*-BN, the natural lattice mismatch of ∼1.8% between the graphene and *h*-BN layers[44,45,51−53] is expected to result in large supercells presenting intricate Moiré patterns.[51] To represent such relaxed supercells, we chose a model consisting of 56 × 56 graphene unit-cells and 55 × 55 *h*-BN unit-cells with L_{CC} = 1.42 Å and L_{BN} = 1.446 Å (see Figure 3a).[51,67,68] We considered rigid shifts of the layers with respect to each other and calculated the RI for each interlayer configuration. The rigidity assumption may be justified by comparing the Young modulii of graphene (∼1.0 TPa)[69,70] and *h*-BN (0.811 TPa)[71] with the corresponding interlayer shear modulii of graphite (4.3−5.1 GPa)[71−73] and *h*-BN (7.7 GPa).[71] We note that a recent theoretical study suggested a dependence of the rigidity of multilayered graphene on the number of layers and predicted a Young modulus as high as 1.4 TPa for bilayer graphene.[74] Furthermore, recent experiments studying the tribology of large graphene flakes indicate that even at the micrometer scale, they are sufficiently rigid to demonstrate superlubric behavior.[75] The resulting RI surface for the relaxed supercell is presented in Figure 3b. As can be seen, the corrugation of the RI surface is ∼0.0055, which is merely 0.55% of the RI difference between the optimal and worst stacking modes of the strained bilayer supercell. From the scaling factor obtained for the strained unit-cell (7.05 meV/atom), we may now estimate the height of the sliding energy barriers in the relaxed supercell to be as low as ∼0.04 meV/atom. Therefore, due to the intrinsic lattice mismatch between graphene and *h*-BN, even in the case of zero interlayer misfit angle, the energy barriers that have to be crossed during the sliding process are very shallow, and superlubricity is expected to occur.

Having explored the corrugation of the sliding surface with respect to lateral shifts, we now turn to study the effect of the interlayer misfit angle on the sliding physics. For this, we consider a finite square graphene flake and align the atom closest to the center of mass of the flake and the atom closest to the center of mass of the *h*-BN supercell exactly atop of each other. Next, we rotate the graphene flake around an axis crossing these two atoms by the required misfit angle (see Figure 4a). Then, we perform lateral shifts of the rotated graphene flake parallel to the armchair axis of the *h*-BN layer and record the amplitude of the RI variations along each such linear path. In the main panel of Figure 4b, this amplitude is plotted as a function of misfit angle for several rectangular graphene flakes of various sizes. For the smallest flake considered (5 × 5), a picture very similar to that obtained for a hexagonal graphene flake sliding on a graphene surface is obtained, where at small misfit angles, the corrugation is high, reducing as the misfit angle increases and increasing again at around $\Phi = 60°$ due to the 6-fold symmetry of the hexagonal lattice.[11,31,59] Upon an increase of the flake size, the overall RI, corrugation reduces monotonously, where for the 56 × 56 graphene flake, the maximum RI corrugation recorded is less than 10% of that calculated for a strained flake (with no graphene/*h*-BN lattice mismatch) of the same dimensions (see the inset of Figure 4b). Using the scaling relation obtained above, the maximal sliding energy corrugation for this flake is estimated to be ∼0.62 meV/atom. We emphasize that even this value is limited to a very narrow region of misfit angles beyond which the sliding RI corrugation becomes negligible for any practical purpose. This indicates that for graphene flakes of

dx.doi.org/10.1021/jz301758c | *J. Phys. Chem. Lett.* 2013, 4, 115−120

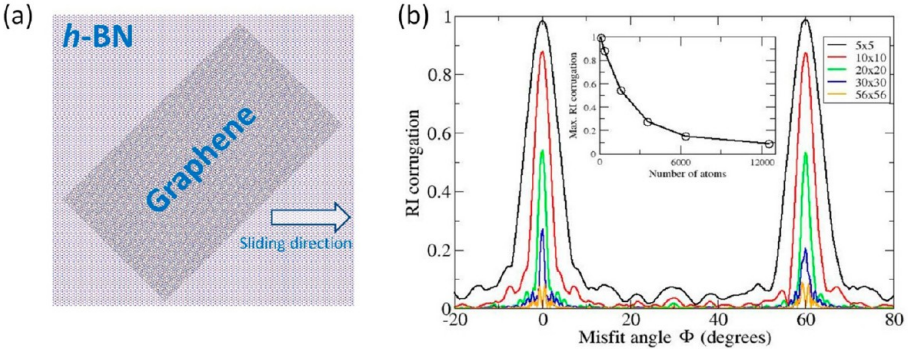

Figure 4. Effect of flake size and misfit angle on the corrugation of the sliding RI surface of the heterogeneous graphene/*h*-BN interface. (a) Schematic representation of a square 56 × 56 graphene flake on top of an *h*-BN layer with a misfit angle of 45°. The sliding direction is marked by the white arrow. (b) Maximal variations of the RI calculated along linear paths in the sliding direction as a function of interlayer misfit angle. (Inset) Maximal RI corrugation as a function of flake size (number of atoms in the flake). The different diagrams presented in panel (b) are normalized to the size of the relevant graphene flake such that a maximal RI corrugation of 1 is obtained for a strained graphene flake consisting of the same number of atoms and geometry having no lattice mismatch with the underlying *h*-BN layer.

appropriate dimensions sliding on top of a *h*-BN layer, the overall sliding friction is expected to be vanishingly small regardless of the relative orientation between the two lattices, thus resulting in a stable superlubric state.

In order to rationalize these results, we recall that the corrugation of the sliding energy landscape in planar layered materials is attributed mainly to the repulsion between overlapping electron clouds around atoms belonging to adjacent layers as they cross each other during the sliding process.[32,33,41,57−59,76−78] The mechanism underlying the occurrence of superlubricity in these microscopic junctions relies on an efficient averaging out and cancellation of such localized forces when the two lattices constructing the contact are incommensurate.[79] For the graphene/*h*-BN junction, the registry mismatch stems not only from the interlayer misfit angle but also from the natural mismatch between the two hexagonal lattices. Therefore, even at small misfit angles, the lattice incommensurability should lower the friction and thus reduce the frictional anisotropy. Nevertheless, because the lattice mismatch is small, the sliding corrugation at low misfit angles is considerably reduced only for sufficiently large flakes where clear Moiré patterns appear.

To summarize, in the present Letter, we have defined the RI of the heterogeneous graphene/*h*-BN interface and used it to characterize the sliding physics of finite graphene flakes on top of *h*-BN layers. We found that for sufficiently large graphene flakes sliding on top of a *h*-BN layer, the overall sliding friction is expected to be vanishingly small regardless of the relative orientation between the two lattices, thus resulting in a stable superlubric state. This is in contrast to the case of the homogeneous graphene interface where flake reorientations are known to eliminate superlubricty. Our results mark heterogeneous layered interfaces, such as the one studied herein, as promising materials for dry lubrication purposes.

■ ASSOCIATED CONTENT

Supporting Information

Detailed description of the geometry and DFT calculations used to study the strained graphene/*h*-BN system. This material is available free of charge via the Internet at http://pubs.acs.org.

■ AUTHOR INFORMATION

Corresponding Author

*E-mail: odedhod@tau.ac.il

Notes

The authors declare no competing financial interest.

■ ACKNOWLEDGMENTS

This work was supported by the Israel Science Foundation under Grant No. 1313/08, the Center for Nanoscience and Nanotechnology at Tel Aviv University, the Israeli Ministry of Defense, and the Lise Meitner-Minerva Center for Computational Quantum Chemistry. The research leading to these results has received funding from the European Community's Seventh Framework Programme FP7/2007-2013 under Grant Agreement No. 249225.

■ REFERENCES

(1) Savage, R. H. Graphite Lubrication. *J. Appl. Phys.* **1948**, *19*, 1−10.
(2) Arnell, R. D.; Teer, D. G. Lattice Parameters of Graphite in Relation to Friction and Wear. *Nature* **1968**, *218*, 1155−1156.
(3) Yen, B. K.; Schwickert, B. E.; Toney, M. F. Origin of Low-Friction Behavior in Graphite Investigated by Surface X-ray Diffraction. *Appl. Phys. Lett.* **2004**, *84*, 4702−4704.
(4) Cohen, S. R.; Rapoport, L.; Ponomarev, E. A.; Cohen, H.; Tsirlina, T.; Tenne, R.; Lévy-Clément, C. The Tribological Behavior of Type II Textured MX_2 (M=Mo, W; X=S, Se) Films. *Thin Solid Films* **1998**, *324*, 190−197.
(5) Rapoport, L.; Fleischer, N.; Tenne, R. Fullerene-Like WS_2 Nanoparticles: Superior Lubricants for Harsh Conditions. *Adv. Mater.* **2003**, *15*, 651−655.
(6) Lee, C.; Li, Q.; Kalb, W.; Liu, X.-Z.; Berger, H.; Carpick, R. W.; Hone, J. Frictional Characteristics of Atomically Thin Sheets. *Science* **2010**, *328*, 76−80.
(7) Donnet, C.; Erdemir, A. Historical Developments and New Trends in Tribological and Solid Lubricant Coatings. *Surf. Coat. Technol.* **2004**, *180−181*, 76−84.
(8) Filleter, T.; McChesney, J. L.; Bostwick, A.; Rotenberg, E.; Emtsev, K. V.; Seyller, T.; Horn, K.; Bennewitz, R. Friction and Dissipation in Epitaxial Graphene Films. *Phys. Rev. Lett.* **2009**, *102*, 086102.
(9) Brown, S.; Musfeldt, J. L.; Mihut, I.; Betts, J. B.; Migliori, A.; Zak, A.; Tenne, R. Bulk vs Nanoscale WS_2: Finite Size Effects and Solid-State Lubrication. *Nano Lett.* **2007**, *7*, 2365−2369.

(10) Graphite on its own is not a good solid lubricant; it requires humidity or low vapor pressure of organic additives to exhibit good lubrication characteristics.
(11) Dienwiebel, M.; Verhoeven, G. S.; Pradeep, N.; Frenken, J. W. M.; Heimberg, J. A.; Zandbergen, H. W. Superlubricity of Graphite. *Phys. Rev. Lett.* **2004**, *92*, 126101.
(12) Dienwiebel, M.; Pradeep, N.; Verhoeven, G. S.; Zandbergen, H. W.; Frenken, J. W. M. Model Experiments of Superlubricity of Graphite. *Surf. Sci.* **2005**, *576*, 197−211.
(13) Hirano, M.; Shinjo, K. Atomistic Locking and Friction. *Phys. Rev. B* **1990**, *41*, 11837.
(14) Shinjo, K.; Hirano, M. Dynamics of Friction: Superlubric State. *Surf. Sci.* **1993**, *283*, 473−478.
(15) Hirano, M.; Shinjo, K.; Kaneko, R.; Murata, Y. Observation of Superlubricity by Scanning Tunneling Microscopy. *Phys. Rev. Lett.* **1997**, *78*, 1448.
(16) Hirano, M. Atomistics of Friction. *Surf. Sci. Rep.* **2006**, *60*, 159−201.
(17) Kim, S. H.; Asay, D. B.; Dugger, M. T. Nanotribology and MEMS. *Nano Today* **2007**, *2*, 22−29.
(18) Bhushan, B.; Israelachvili, J. N.; Landman, U. Nanotribology: Friction, Wear and Lubrication at the Atomic Scale. *Nature* **1995**, *374*, 607−616.
(19) Urbakh, M.; Klafter, J.; Gourdon, D.; Israelachvili, J. The Nonlinear Nature of Friction. *Nature* **2004**, *430*, 525−528.
(20) Frenken, J. Nanotribology: Bringing Friction to a Halt. *Nat. Nano* **2006**, *1*, 20−21.
(21) Cumings, J.; Zettl, A. Low-Friction Nanoscale Linear Bearing Realized from Multiwall Carbon Nanotubes. *Science* **2000**, *289*, 602−604.
(22) Grierson, D. S.; Carpick, R. W. Nanotribology of Carbon-Based Materials. *Nano Today* **2007**, *2*, 12−21.
(23) Kis, A.; Jensen, K.; Aloni, S.; Mickelson, W.; Zettl, A. Interlayer Forces and Ultralow Sliding Friction in Multiwalled Carbon Nanotubes. *Phys. Rev. Lett.* **2006**, *97*, 025501.
(24) Buldum, A.; Lu, J. P. Atomic Scale Sliding and Rolling of Carbon Nanotubes. *Phys. Rev. Lett.* **1999**, *83*, 5050.
(25) Falvo, M. R.; Taylor Ii, R. M.; Helser, A.; Chi, V.; Brooks, F. P., Jr.; Washburn, S.; Superfine, R. Nanometre-Scale Rolling and Sliding of Carbon Nanotubes. *Nature* **1999**, *397*, 236−238.
(26) Sheehan, P. E.; Lieber, C. M. Nanotribology and Nanofabrication of MoO_3 Structures by Atomic Force Microscopy. *Science* **1996**, *272*, 1158−1161.
(27) Forró, L. Beyond Gedanken Experiments. *Science* **2000**, *289*, 560−561.
(28) Shirai, Y.; Osgood, A. J.; Zhao, Y.; Kelly, K. F.; Tour, J. M. Directional Control in Thermally Driven Single-Molecule Nanocars. *Nano Lett.* **2005**, *5*, 2330−2334.
(29) Zheng, Q.; Jiang, B.; Liu, S.; Weng, Y.; Lu, L.; Xue, Q.; Zhu, J.; Jiang, Q.; Wang, S.; Peng, L. Self-Retracting Motion of Graphite Microflakes. *Phys. Rev. Lett.* **2008**, *100*, 067205.
(30) Tomlinson, G. A. CVI. A Molecular Theory of Friction. *Philos. Mag., Ser. 7* **1929**, *7*, 905−939.
(31) Verhoeven, G. S.; Dienwiebel, M.; Frenken, J. W. M. Model Calculations of Superlubricity of Graphite. *Phys. Rev. B* **2004**, *70*, 165418.
(32) Kolmogorov, A. N.; Crespi, V. H. Registry-Dependent Interlayer Potential for Graphitic Systems. *Phys. Rev. B* **2005**, *71*, 235415.
(33) Marom, N.; Bernstein, J.; Garel, J.; Tkatchenko, A.; Joselevich, E.; Kronik, L.; Hod, O. Stacking and Registry Effects in Layered Materials: The Case of Hexagonal Boron Nitride. *Phys. Rev. Lett.* **2010**, *105*, 046801.
(34) Björk, J.; Hanke, F.; Palma, C.-A.; Samori, P.; Cecchini, M.; Persson, M. Adsorption of Aromatic and Anti-Aromatic Systems on Graphene through $\pi-\pi$ Stacking. *J. Phys. Chem. Lett.* **2010**, *1*, 3407−3412.
(35) Hod, O. Graphite and Hexagonal Boron-Nitride Have the Same Interlayer Distance. Why? *J. Chem. Theory Comput.* **2012**, *8*, 1360−1369.
(36) Marom, N.; Tkatchenko, A.; Rossi, M.; Gobre, V. V.; Hod, O.; Scheffler, M.; Kronik, L. Dispersion Interactions with Density-Functional Theory: Benchmarking Semiempirical and Interatomic Pairwise Corrected Density Functionals. *J. Chem. Theory Comput.* **2011**, *7*, 3944−3951.
(37) Björkman, T.; Gulans, A.; Krasheninnikov, A. V.; Nieminen, R. M. van der Waals Bonding in Layered Compounds from Advanced Density-Functional First-Principles Calculations. *Phys. Rev. Lett.* **2012**, *108*, 235502.
(38) de Wijn, A. S.; Fusco, C.; Fasolino, A. Stability of Superlubric Sliding on Graphite. *Phys. Rev. E* **2010**, *81*, 046105.
(39) de Wijn, A. S.; Fasolino, A.; Filippov, A. E.; Urbakh, M. Low Friction and Rotational Dynamics of Crystalline Flakes in Solid Lubrication. *Europhys. Lett.* **2011**, *95*, 66002.
(40) Filippov, A. E.; Dienwiebel, M.; Frenken, J. W. M.; Klafter, J.; Urbakh, M. Torque and Twist against Superlubricity. *Phys. Rev. Lett.* **2008**, *100*, 046102.
(41) Kolmogorov, A. N.; Crespi, V. H. Smoothest Bearings: Interlayer Sliding in Multiwalled Carbon Nanotubes. *Phys. Rev. Lett.* **2000**, *85*, 4727.
(42) Smolyanitsky, A.; Killgore, J. P.; Tewary, V. K. Effect of Elastic Deformation on Frictional Properties of Few-Layer Graphene. *Phys. Rev. B* **2012**, *85*, 035412.
(43) Nikiforov, I.; Tang, D.-M.; Wei, X.; Dumitrică, T.; Golberg, D. Nanoscale Bending of Multilayered Boron Nitride and Graphene Ribbons: Experiment and Objective Molecular Dynamics Calculations. *Phys. Rev. Lett.* **2012**, *109*, 025504.
(44) Giovannetti, G.; Khomyakov, P. A.; Brocks, G.; Kelly, P. J.; van den Brink, J. Substrate-Induced Band Gap in Graphene on Hexagonal Boron Nitride: Ab Initio Density Functional Calculations. *Phys. Rev. B* **2007**, *76*, 073103.
(45) Dean, C. R.; Young, A. F.; Meric, I.; Lee, C.; Wang, L.; Sorgenfrei, S.; Watanabe, K.; Taniguchi, T.; Kim, P.; Shepard, K. L.; Hone, J. Boron Nitride Substrates for High-Quality Graphene Electronics. *Nat. Nano* **2010**, *5*, 722−726.
(46) Slawinska, J.; Zasada, I.; Klusek, Z. Energy Gap Tuning in Graphene on Hexagonal Boron Nitride Bilayer System. *Phys. Rev. B* **2010**, *81*, 155433.
(47) Sławinska, J.; Zasada, I.; Kosinski, P.; Klusek, Z. Reversible Modifications of Linear Dispersion: Graphene between Boron Nitride Monolayers. *Phys. Rev. B* **2010**, *82*, 085431.
(48) Ding, X.; Ding, G.; Xie, X.; Huang, F.; Jiang, M. Direct Growth of Few Layer Graphene on Hexagonal Boron Nitride by Chemical Vapor Deposition. *Carbon* **2011**, *49*, 2522−2525.
(49) Fan, Y.; Zhao, M.; Wang, Z.; Zhang, X.; Zhang, H. Tunable Electronic Structures of Graphene/Boron Nitride Heterobilayers. *Appl. Phys. Lett.* **2011**, *98*, 083103−083103.
(50) Liu, Z.; Song, L.; Zhao, S.; Huang, J.; Ma, L.; Zhang, J.; Lou, J.; Ajayan, P. M. Direct Growth of Graphene/Hexagonal Boron Nitride Stacked Layers. *Nano Lett.* **2011**, *11*, 2032−2037.
(51) Sachs, B.; Wehling, T. O.; Katsnelson, M. I.; Lichtenstein, A. I. Adhesion and Electronic Structure of Graphene on Hexagonal Boron Nitride Substrates. *Phys. Rev. B* **2011**, *84*, 195414.
(52) Xue, J.; Sanchez-Yamagishi, J.; Bulmash, D.; Jacquod, P.; Deshpande, A.; Watanabe, K.; Taniguchi, T.; Jarillo-Herrero, P.; LeRoy, B. J. Scanning Tunnelling Microscopy and Spectroscopy of Ultra-Flat Graphene on Hexagonal Boron Nitride. *Nat. Mater.* **2011**, *10*, 282−285.
(53) Yankowitz, M.; Xue, J.; Cormode, D.; Sanchez-Yamagishi, J. D.; Watanabe, K.; Taniguchi, T.; Jarillo-Herrero, P.; Jacquod, P.; LeRoy, B. J. Emergence of Superlattice Dirac Points in Graphene on Hexagonal Boron Nitride. *Nat. Phys.* **2012**, *8*, 382−386.
(54) Ponomarenko, L. A.; Geim, A. K.; Zhukov, A. A.; Jalil, R.; Morozov, S. V.; Novoselov, K. S.; Grigorieva, I. V.; Hill, E. H.; Cheianov, V. V.; Falko, V. I.; Watanabe, K.; Taniguchi, T.; Gorbachev, R. V. Tunable Metal−Insulator Transition in Double-Layer Graphene Heterostructures. *Nat. Phys.* **2011**, *7*, 958−961.
(55) Decker, R. g.; Wang, Y.; Brar, V. W.; Regan, W.; Tsai, H.-Z.; Wu, Q.; Gannett, W.; Zettl, A.; Crommie, M. F. Local Electronic

Properties of Graphene on a BN Substrate via Scanning Tunneling Microscopy. *Nano Lett.* **2011**, *11*, 2291−2295.
(56) Meric, I.; Dean, C.; Young, A.; Hone, J.; Kim, P.; Shepard, K. L.Graphene field-effect transistors based on boron nitride gate dielectrics. *Tech. Digest Int. Electron Devices Meet.* 2010, *10*, 556−559.
(57) Hod, O. Quantifying the Stacking Registry Matching in Layered Materials. *Isr. J. Chem.* **2010**, *50*, 506−514.
(58) Blumberg, A.; Keshet, U.; Zaltsman, I.; Hod, O. Interlayer Registry to Determine the Sliding Potential of Layered Metal Dichalcogenides: The Case of 2*H*-MoS_2. *J. Phys. Chem. Lett.* **2012**, *3*, 1936−1940.
(59) Hod, O. Interlayer Commensurability and Superlubricity in Rigid Layered Materials. *Phys. Rev. B* **2012**, *86*, 075444.
(60) Heyd, J.; Scuseria, G. E.; Ernzerhof, M. Hybrid Functionals Based on a Screened Coulomb Potential. *J. Chem. Phys.* **2003**, *118*, 8207−8215.
(61) Heyd, J.; Scuseria, G. E. Assessment and Validation of a Screened Coulomb Hybrid Density Functional. *J. Chem. Phys.* **2004**, *120*, 7274−7280.
(62) Heyd, J.; Scuseria, G. E. Efficient Hybrid Density Functional Calculations in Solids: Assessment of the Heyd−Scuseria−Ernzerhof Screened Coulomb Hybrid Functional. *J. Chem. Phys.* **2004**, *121*, 1187−1192.
(63) Hariharan, P. C.; Pople, J. A. The Influence of Polarization Functions on Molecular Orbital Hydrogenation Energies. *Theor. Chem. Acc.* **1973**, *28*, 213−222.
(64) Frisch, M. J.; et al. *Gaussian 09*, revision A.02; Gaussian Inc.: Wallingford, CT, 2009.
(65) Barone, V.; Hod, O.; Peralta, J. E.; Scuseria, G. E. Accurate Prediction of the Electronic Properties of Low-Dimensional Graphene Derivatives Using a Screened Hybrid Density Functional. *Acc. Chem. Res.* **2011**, *44*, 269−279.
(66) Park, H.; Wadehra, A.; Wilkins, J. W.; Neto, A. H. C. Magnetic States and Optical Properties of Single-Layer Carbon-Doped Hexagonal Boron Nitride. *Appl. Phys. Lett.* **2012**, *100*, 253115.
(67) For simplicity, instead of the hexagnal unit-cells of graphene and *h*-BN containing two atoms each, we consider four-atom rectangular unit-cells and use them to construct the rectangular bilayer supercell.
(68) As the interactions responsible for the corrugated sliding energy landscape are of short-range nature, the periodic bilayer supercell is replaced by finite flakes of the same dimensions where extra margins are added to the *h*-BN model so that upon shifting of the graphene flake, it does not slide beyond its edges.
(69) Bosak, A.; Krisch, M.; Mohr, M.; Maultzsch, J.; Thomsen, C. Elasticity of Single-Crystalline Graphite: Inelastic X-ray Scattering Study. *Phys. Rev. B* **2007**, *75*, 153408.
(70) Lee, C.; Wei, X.; Kysar, J. W.; Hone, J. Measurement of the Elastic Properties and Intrinsic Strength of Monolayer Graphene. *Science* **2008**, *321*, 385−388.
(71) Bosak, A.; Serrano, J.; Krisch, M.; Watanabe, K.; Taniguchi, T.; Kanda, H. Elasticity of Hexagonal Boron Nitride: Inelastic X-ray Scattering Measurements. *Phys. Rev. B* **2006**, *73*, 041402.
(72) Tan, P. H.; Han, W. P.; Zhao, W. J.; Wu, Z. H.; Chang, K.; Wang, H.; Wang, Y. F.; Bonini, N.; Marzari, N.; Pugno, N.; Savini, G.; Lombardo, A.; Ferrari, A. C. The Shear Mode of Multilayer Graphene. *Nat. Mater.* **2012**, *11*, 294−300.
(73) Grimsditch, M. Shear Elastic Modulus of Graphite. *J. Phys. C: Solid State Phys.* **1983**, *16*, L143.
(74) Zhang, D. B.; Akatyeva, E.; Dumitrică, T. Bending Ultrathin Graphene at the Margins of Continuum Mechanics. *Phys. Rev. Lett.* **2011**, *106*, 255503.
(75) Liu, Z.; Yang, J.; Grey, F.; Liu, J. Z.; Liu, Y.; Wang, Y.; Yang, Y.; Cheng, Y.; Zheng, Q. Observation of Microscale Superlubricity in Graphite. *Phys. Rev. Lett.* **2012**, *108*, 205503.
(76) Sun, C. Q.; Tay, B. K.; Lau, S. P.; Sun, X. W.; Zeng, X. T.; Li, S.; Bai, H. L.; Liu, H.; Liu, Z. H.; Jiang, E. Y. Bond Contraction and Lone Pair Interaction at Nitride Surfaces. *J. Appl. Phys.* **2001**, *90*, 2615−2617.
(77) Liang, T.; Sawyer, W. G.; Perry, S. S.; Sinnott, S. B.; Phillpot, S. R. First-Principles Determination of Static Potential Energy Surfaces for Atomic Friction in MoS_2 and MoO_3. *Phys. Rev. B* **2008**, *77*, 104105.
(78) Sun, C. Q.; Sun, Y.; Ni, Y.; Zhang, X.; Pan, J.; Wang, X.-H.; Zhou, J.; Li, L.-T.; Zheng, W.; Yu, S.; Pan, L. K.; Sun, Z. Coulomb Repulsion at the Nanometer-Sized Contact: A Force Driving Superhydrophobicity, Superfluidity, Superlubricity, and Supersolidity. *J. Phys. Chem. C* **2009**, *113*, 20009−20019.
(79) Hirano, M. Superlubricity: A State of Vanishing Friction. *Wear* **2003**, *254*, 932−940.